sustainability

MDPI

Article

Assessment of the Mechanical Properties of High Strength Mortar Incorporating Silica Fume and Graphene Nanoplatelets: Experimental and Mathematical Modeling

Husam A. Salah [1,*], Azrul A. Mutalib [1,*], Hassan Amer Algaifi [2], Iskandar Bin Yahya [3], M. A. I. Yusof [1], Nazmus Sakib [1] and Mohamed Elsayed [1]

[1] Department of Civil Engineering, Faculty of Engineering and Built Environment, Universiti Kebangsaan Malaysia (UKM), Bangi 43600, Malaysia
[2] Institute of Energy Infrastructure (IEI), Universiti Tenaga Nasional, Jalan IKRAM-UNITEN, Kajang 43000, Malaysia
[3] Department of Electrical, Electronics and Systems Engineering, Faculty of Engineering and Built Environment, Universiti Kebangsaan Malaysia (UKM), Bangi 43600, Malaysia
* Correspondence: p97967@siswa.ukm.edu.my (H.A.S.); azrulaam@ukm.edu.my (A.A.M.)

Abstract: Cement-based mortar is recognized as a popular and cost-effective material for the rehabilitation and repair of reinforced concrete structures. However, the development of high-performance cement-based mortar is in high demand in order to not only enhance compressive strength but also to prolong the mortar lifespan and minimize maintenance costs as much as possible. In the current study, high-strength mortars incorporating both silica fume and graphene nanoplatelets (GNPs) were investigated and evaluated based on compressive and flexural strength. The graphene powder was added in amounts ranging from 0.5% to 2%, by cement weight, while silica fume was added as a partial replacement for cement (10%). The optimal content of the graphene was determined using response surface methodology (RSM). In addition, field emission scanning electron microscopy (FESEM) was used to assess the proposed mortar at the micro-scale level. The outcome revealed that the graphene-based mortar imparted superior mechanical properties compared to the control mixture. The compressive and flexural strength of the mortars containing 10% silica fume and 1% graphene increased by 33% and 35%, respectively. This positive result was attributed to the refinement of the nanopores and tiny cracks by the inclusion of GNPs, which was supported by microstructure testing. The RSM model was also shown to be capable of optimizing and predicting compressive and flexural strength with less error. It is possible to conclude that graphene-based high-strength mortar will serve as a sustainable material in the near future.

Keywords: high-strength mortar; graphene-based mortar; cementitious material; compressive strength; graphene nanoplatelets

Citation: Salah, H.A.; Mutalib, A.A.; Algaifi, H.A.; Yahya, I.B.; Yusof, M.A.I.; Sakib, N.; Elsayed, M. Assessment of the Mechanical Properties of High Strength Mortar Incorporating Silica Fume and Graphene Nanoplatelets: Experimental and Mathematical Modeling. *Sustainability* **2023**, *15*, 8054. https://doi.org/10.3390/su15108054

Academic Editor: Tommaso Caloiero

Received: 17 March 2023
Revised: 14 April 2023
Accepted: 25 April 2023
Published: 15 May 2023

1. Introduction

Cement-based mortar is one of the most commonly used materials for the rehabilitation and repair of reinforced concrete structures [1]. Despite its good compressive strength and low cost, it has several drawbacks, including the presence of micropores, the inevitable formation of microcracks, and low flexural and tensile strength [2]. These undesirable characteristics can shorten the lifespan of mortar and necessitate extensive maintenance, ultimately limiting its use in the construction industry. Therefore, the civil engineering community shifted their attention to developing high-performance mortar through different approaches. Traditional approaches, such as lowering the water/cement ratio, were adopted to minimize capillary and gel pores in the past [3]. Other researchers tried to incorporate steel fiber in a cement mortar mixture, which substantially enhances structural features, such as flexural strength and tensile strength [4]. It was found that the mechanical

properties of mortar that incorporated steel fiber significantly improved compared to that of the control mixture [5]. However, including, steel fibers at higher dosages has some disadvantages in terms of higher costs and poor workability. Furthermore, voids and honeycombs may form during the steel fibers' placement, owing to the improper compaction and the high stiffness of the steel fibers in the mixture [6].

The use of rich silica-based materials (pozzolanic materials), such as fly ash, silica fume, and slag, as partial replacements for cement, has also received much attention regarding densifying the mortar structure at the micro-scale level. When compared to control mortar, the silica-based material imparted superior mechanical and durability properties [7]. However, the inclusion of pozzolanic material is not enough to improve the quality and durability of mortar at the nanoscale level. For instance, Al-Jabri and Shoukry [8] suggested incorporating nano-sized particles of a size below 300 nm in order to improve strength and durability properties. The results showed that the compressive strength of nanostructured blended mortar is greater than that of plain mortar, with an increase of approximately 33% observed. Rao, Silva [9], in turn, used nano titanium (nano TiO_2) and nano silica (nano SiO_2) to develop self-compacting mortar with less porosity. The findings indicate that implementing nanomaterials in the rehabilitation and repair of mortars has a lot of potential. When compared to the control mixture, the use of nano-sized cement kiln dust as a partial replacement for cement raised the compressive strength of the cement mortar by about 15–30% [10]. This fact is in line with Wang Dong [11], who demonstrated that nanofillers can improve the bond strength and interfacial microstructures between aggregates and cement mortars. Regardless, these nanofiller materials might have relatively high costs and some environmental concerns during their preparation, which are regarded as weaknesses and limit their application. As a result, many researchers have shifted their focus in recent years to using alternative nanomaterials, such as graphene, to improve mortar quality. This is due to the fact that graphene is easier to obtain, more renewable, and less expensive compared to other nanomaterials [12].

Graphene ($C_{24}H_{24}$) is a two-dimensional carbon nanomaterial with a tensile strength of up to 130 GPa, making it one of the strongest materials [13]. Several graphene derivatives were used in reinforcing cementitious materials, such as graphene oxide, reduced graphene oxide, and graphene nanoplatelets [14]. Li et al. [15] evaluated graphene oxide ($C_{54}H_{17}$ + O+$(OH)_3$ + COOH) incorporated mortar. The findings revealed that the tensile splitting and flexural strength were improved by about 15%, while the compressive strength was significantly enhanced by more than 25%. This is in agreement with Wang Wang [16], who recorded an improvement in the flexural strength of mortar owing to the presence of graphene oxide. Despite the benefits of graphene oxide (GO) in cement mortar, an excess of oxygen functional groups in GO would trigger undesirable issues inside cement-based concrete. This is because both the negative charge of GO and the positive charge of Ca^{2+}, Na^+, and K^+ existing inside the cement matrix tend to agglomerate due to van der Waals forces [17]. The increased formation of agglomerates may result in the formation of a weak zone within the concrete matrix. Therefore, some researchers shifted their attention to using reduced graphene oxide [18,19], while others used graphene powder to improve cementitious materials instead of GO [20,21].

It can be seen that many researchers adopted different approaches to improve the properties of normal cement mortar, such as using nano-silica, graphene oxide, and so on, while limited research has involved using Graphene Nanoplatelets to enhance high-strength mortar. Furthermore, no optimization model exists to predict and optimize the optimal content of Graphene Nanoplatelets in high-strength mortar. Herein, the compressive and flexural strengths of high-strength mortar incorporating both silica fume and Graphene Nanoplatelets were investigated and evaluated. Field emission scanning electron microscopy (FESEM) was also used to assess the microstructure of the proposed mortar. The optimal GNPs content in the high-strength mortar was also determined using optimization modeling based on response surface methodology.

2. Materials and Theoretical Program

2.1. Materials

Materials used for the proposed high-strength mortar preparation include graphene, cement, slice fume, fine aggregate, water, and superplasticizer. The graphene used for this experiment is GNPs. It was purchased from GrapheneCA Inc. (New York, NY, USA). Figure 1 shows the morphology of graphene. Ordinary Portland cement class l 52.5 was used in this study, while silica fume was collected from a local supplier. The chemical composition of the cement and silica fume is presented in Table 1, which was determined using X-ray fluorescence (XRF) spectroscopy. The particle size distribution of cement, silica fume, and fine aggregate was determined and analyzed using a laser diffraction particle size analyzer, as shown in Figure 2. It can be seen that the silica fume particles are finer than cement and sand particles. A natural local sand was also used as fine aggregate. To increase the workability of the concrete mix, a superplasticizer (1% by cement weight) was used.

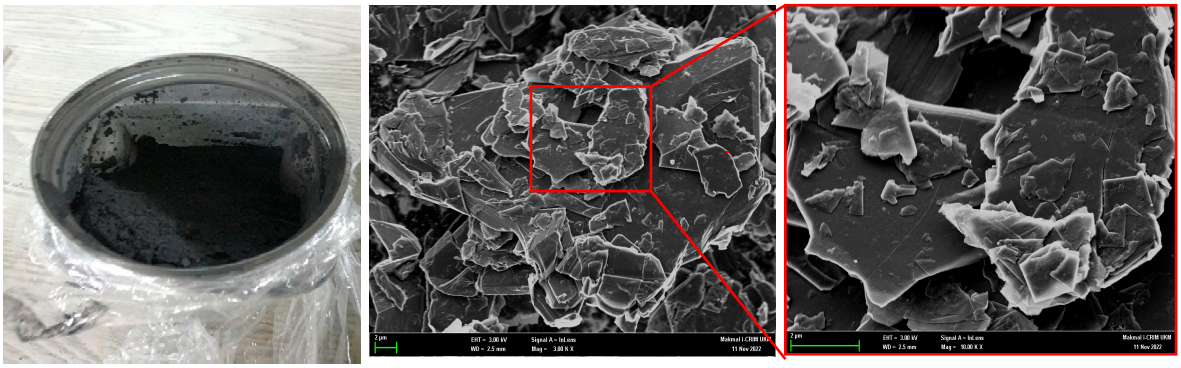

Figure 1. Morphology of GNPs.

Table 1. Chemical composition of cement and silica fume used in the present study.

Constituents	Mass Percentage %	
	Silica Fume	Cement
SiO_2	96.00	15.9
CaO	0.27	69.8
Al_2O_3	0.72	3.43
MgO	0.40	0.991
SO_3	0.19	4.32
Fe_2O_3	0.10	3.93
K_2O	0.83	0.94
Na_2O	0.26	0.0773
Others	0.20	n/a
LOI	1.00	n/a

Note: n/a represents the not applicable data.

2.2. Mix Design Proportions

Table 2 shows the mixed proportions of the control mortar (without graphene), which had a cement-to-sand ratio of 1:1.5 by mass and a water-cement ratio of 0.32. The proportions of the graphene-based mortar were similar to the control mix, with the addition of graphene and silica fume. The graphene powder was added within the range of 0.5% to 0.2% by weight of the total binder, while SF was added as a partial replacement for cement (20% by wt.) and kept constant across all mixes. Furthermore, the superplasticizer dosage ranged from 0.5% to 1.5% (by cement weight) in order to keep the water content constant across all mixes, which is helpful for future comparison and evaluation. Using the flow table shown in Figure 3, it was discovered that the workability of the mortar was 167 mm. It is of note that the flow test was carried out in accordance with ASTM C1437 and ASTM C230 [22,23].

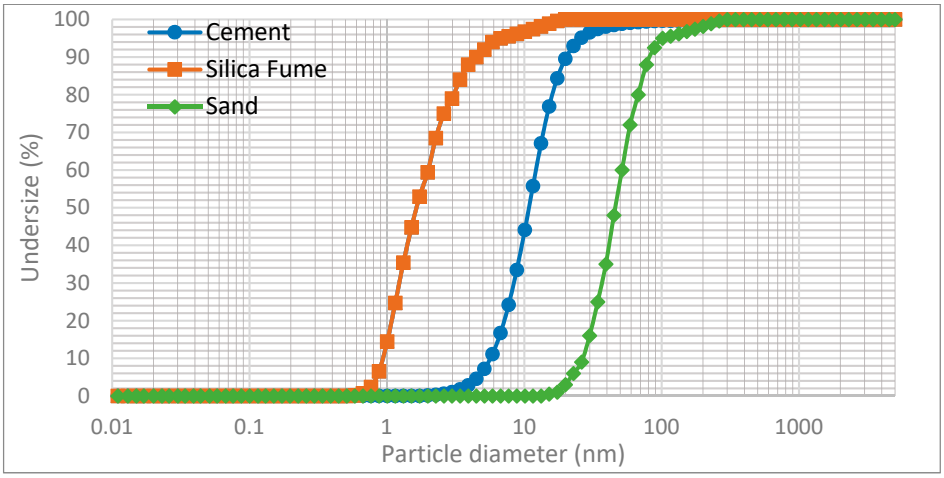

Figure 2. Particle size distribution for cement, silica fume, and sand.

Table 2. Materials proportions of control and graphene-based mortar.

Mix Code No.	Mixes (%) GNPs	Cement (kg/m^3)	Silica Fume (kg/m^3)	GNPs (kg/m^3)	Water (kg/m^3)	Fine Aggregate (kg/m^3)	Superplasticizer 1% (kg/m^3)
C1	0	827	0	0.00	266.80	1241	7.44
C2	0	744	83	0.00	266.80	1241	7.44
M1	0.5	740.30	83	3.70	266.80	1241	7.44
M2	1	736.56	83	7.44	266.80	1241	7.44
M3	1.5	732.84	83	11.16	266.80	1241	7.44
M4	2	729.12	83	14.88	266.80	1241	7.44

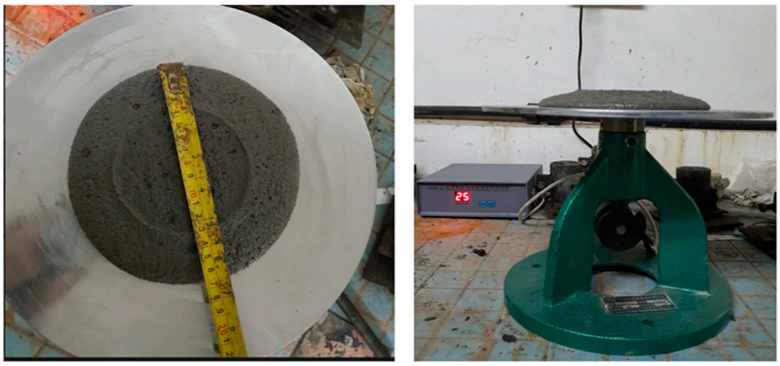

Figure 3. Workability of graphene-based mortar using flow table.

For all mixes, the mortar was mixed using the same procedure. In the first step, both SF and cement were mixed for 1 min at low speed to ensure binder homogeneity. After that, the fine aggregate was added to the binder and was mixed for 1 min. After that, a solution containing GNPs, mixing water, and superplasticizer was gradually added to the dry mortar and mixed for another 2 min at a higher speed. After casting the fresh mortar into the target steel molds, vibration was applied for 1 min to remove air voids. After 24 h, the hardened mortar was removed from the target steel molds and stored inside a water tank for curing.

2.3. Compressive Strength Test

The compressive strengths of graphene-based mortar and a control mix were determined at interval times. The test was performed in accordance with ASTM C109-109M. A cubic sample with a size of 50 × 50 × 50 mm was used in triplicate. According to the standard, the cubic sample was prepared and placed on the compression machine. After

that, the samples were subjected to a constant load (1000 N/s) until they failed, and then the results were recorded. Equation (5) was used to calculate the cubic compressive strength (*CS*) in MPa, using the measured failure load. Here, *A* denotes the cubic sample area in mm^2 and *P* denotes the total applied load in N.

$$CS = \frac{P}{A} \tag{1}$$

2.4. Flexural Strength Test

The flexural strengths of the graphene-based mortar and control mix were determined using ASTM C 348. At the ages of 3, 7, 14, and 28 days, cured prism beams with dimensions of 40 × 40 × 160 mm were subjected to center point loading. The distance between the two support rollers was 120 mm. The loading rate was 50 N/s, and Equation (6) were used to calculate the flexural strength (*FS*) in MPa. It should be noted that triplicate specimens were used, and the average was used for evaluation.

$$FS = 0.0028\ P \tag{2}$$

2.5. Microstructure Test

The scanning electron microscope (SEM-EDX) was used to examine the morphology of the mortar mix at the microstructure level and to identify the chemical product within the mortar. After undergoing a compression test at the age of 28 days, a small specimen (less than 10 mm) was extracted from the cubic sample. The specimen was then dried in an oven at 60 degrees Celsius to remove the moisture content before the SEM test. Prior to scanning, these specimens were coated with gold to improve the resolution. The sample was scanned using ZEISS MERLIN Field Emission Scanning Electron Microscopes outfitted with an energy-dispersive X-ray analyzer.

2.6. Optimization Modelling

Response surface methodology (RSM) is widely used as an experimental design approach for optimization purposes. RSM has also been recognized as a reliable optimization technique in previous research works. This is because it can effectively evaluate the significant interactions between dependent variables and independent variables. In addition, it involves the combination of both statistical and mathematical methods which enable it to achieve its goal with high accuracy. The experimental design approach utilized in the study was a face-centered central composite design (FC-CCD), which is a type of response surface methodology. The FC-CCD followed a five-step process, beginning with determining the number of experiments. The experimental data collected in the second step were analyzed using the software Design-Expert or Minitab. Then, a developed equation was used to construct a numerical model. After that, the accuracy and performance of the model were verified through analysis of variance (ANOVA). In the final step, the desirability function was employed to determine the optimum value.

In particular, herein, the response surface methodology is used to optimize the independent variables, such as GNPs content (X_1) and time (X_2), based on the highest values of the dependent variables (Y_i), including the compressive strength (*CS*) and flexural strength (FS) of the mortar. RSM can also accurately predict and optimize cement-based materials' properties. Herein, the RSM optimization model was created using Design Expert software (Version 13, Minneapolis, MN 55413, USA). It should be noted that the RSM model was created using a face-centered central composite design (FC-CCD), as illustrated in Table 3. As can be seen, the highest graphene content was 2%, while the lowest was 0.5%. Similarly, the longest curing time was 28 days, while the shortest curing time was 3 days.

Table 3. The suggested design of the experimental test according to FC-CCD-RSM.

No. of Experiment	(Independent Variables)		Coded Values	
	GNPs (%)	Time (Days)	Low	High
Mix 1	0.5	3	−1	−1
Mix 2	0.5	15	−1	0
Mix 3	0.5	28	−1	1
Mix 4	1.25	3	0	−1
Mix 5	1.25	15	0	0
Mix 6	1.25	28	0	1
Mix 7	2	3	1	−1
Mix 8	2	15	1	0
Mix 9	2	28	1	1

In the same context, the relationship between the dependent and independent variables was determined using a second-order polynomial equation (quadratic equation). The general form of the quadratic equation is represented in Equation (1), where b_{ii} denotes the quadratic coefficients, b_o corresponds to the intercept of the model, and b_i denotes the linear coefficients [2]. The accuracy and reliability of the developed quadratic equations were verified using several mathematical and statistical tests. The analysis of variance (ANOVA) is one of the best statistical tools to assess the optimization model's performance. The best performance is achieved when the F-value is high while the *p*-value is less than 0.05 [24]. The coefficient of determination (R^2) is also used to evaluate the closeness results between the actual and predicted results, as shown in Equation (2). Where Y_p and Y_a represent the predicted and experimental output, respectively, denotes the average experimental outcome. In addition, the reliability and accuracy of the proposed equation were also evaluated using mean absolute percentage error (*MAPE*) and scatter index (*SI*), as shown in Equations (3) and (4).

$$Y = \beta_o + \sum_{i=1}^{k} \beta_i X_i + \sum_{i=1}^{k} \beta_{ii} X_i^2 + \sum_{i=1}^{k} \beta_{ij} X_{ij} \quad (3)$$

$$R^2 = \frac{\sum_{i=1}^{n} \left(Y_p - \bar{Y_a} \right)^2}{\sum_{i=1}^{n} \left(\bar{Y_a} - Y_a \right)^2} \quad (4)$$

$$MAPE = \frac{1}{n} \sum_{i=1}^{n} \left| \frac{Y_a - Y_p}{Y_a} \right| \quad (5)$$

$$SI = \frac{\sqrt{\frac{1}{n} \sum_{i=1}^{n} \left(Y_a - Y_p \right)^2}}{\bar{Y_a}} \quad (6)$$

3. Results and Discussion

3.1. Mechanical Properties Analysis

Figure 4 presents both the experimental and predicted compressive and flexural strengths of the mortar containing GNPs and silica fume at 3, 7, 14, and 28 days. For the predicted results, two quadratic equations (12 and 13) were developed to predict the compressive and flexural strength. The accuracy of the equations was proved using MAPE and *SI*, whereas the closeness between the experimental and the anticipated results were validated using R^2. In particular, the values of MAPE and *SI* were close to zero (less than 0.1034) for all equations, confirming that the equations are reliable and robust. In addition, R^2 was greater than 0.97, indicating that a strong correlation was achieved, as shown in

Figure 1. This is in line with Carrillo, Ramirez [25], who stated that when the R^2 value is between 0.8 and 1, the model is accurate. Furthermore, no error was recorded in the data as the residual error was evenly distributed across the entire data range.

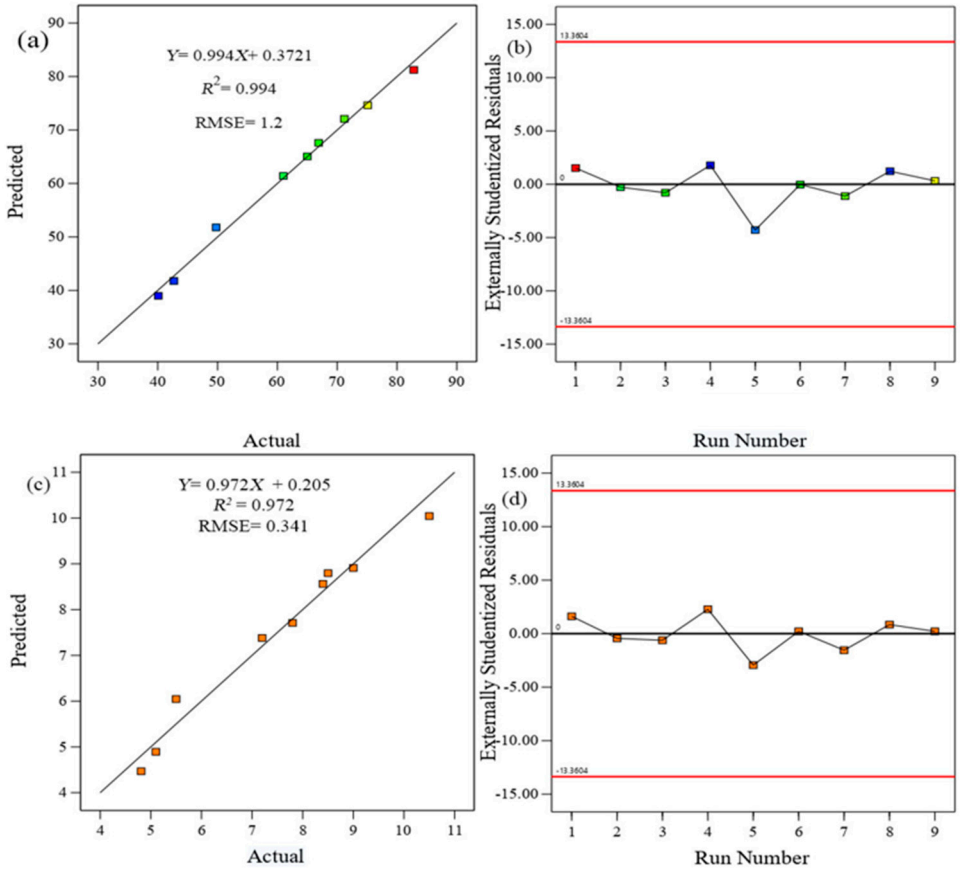

Figure 4. Correlation between the actual and predicted: (**a**) compressive strength; (**b**) compressive strength; (**c**) flexural strength; (**d**) flexural strength.

The difference between the predicted R^2 and adjusted R^2 was also found to be less than 0.2, confirming that the model had the ability to future usage with minimal errors. forecast further usage with low error. This fact was also in agreement with Mohammed Khed [26]. Furthermore, the value of the adjusted R^2 was close to R^2, indicating that the variables did not affect the model's performance. The significance of the predicted equations was also proven using Adeq precision, in which its value was more significant than 27.9. This result is in line with Gong Song [27], who demonstrated that the desirable model is achieved when the added precision value is greater than 4.0. The applicability of the proposed optimization equation was also assessed using the F-value and *p*-value, which can be considered significant when the *p*-value is less than 0.005 and F-value is high. For this RSM model, the F-value of the model was greater than 99.71 while the *p*-value was 0.0016, which confirmed that the developed model was significant. This fact was also consistent with previous studies. For example, the predicted equation of the early age compressive strength of magnesium phosphate cement-based material was verified using the F-value and the *p*-value in a study by Hou Chen [28]. In the outcome of their study, the F-value and *p*-value were 21.29 and 0.0003, respectively, highlighting that the model was significant.

$$CS = 74.63 + 1.82X_1 + 14.73X_2 + 0.43X_1X_2 - 11.4X_1^2 - 8.12X_2^2 \quad (7)$$

$$FS = 8.91 + 0.165X_1 + 2X_2 - 0.048X_1X_2 - 1.37X_1^2 - 0.86X_2^2 \quad (8)$$

It is important to note that the experimental results were presented using a bar chart, while a contour plot was constructed using the above quadratic equations to present the predicted strength. The red region represents the highest value, while the blue represents the lowest compressive strength. Prediction and actual compressive strength show that all of the mixes strengths increased with increasing their age. For example, the percentage increment of the compressive strength (Figure 5a) of the mortar incorporating 1% GNPs at 28 days was 83.3 MPa higher than at the age of 3 days (50 MPa). Similarly, the flexural strength (Figure 5b) increment percentage of the mortar containing 1% graphene was 10.8 MPa greater than at the age of 3 days (6.5 MPa). It is also important to note that the compressive strength increased significantly with increasing the graphene content up to almost 1.5%. Beyond this value, there is a slight drop in compressive and flexural strength. This is in line with Sajjad Sheikh [20], who found that the optimum content of GNPs was 1% if intended to enhance geopolymer mortar's compressive strength. In general, the enhancement of the mortar containing the graphene and silica fume was attributed to two reasons. The first reason was due to the refinement of pores by silica fume, as it produces further gel product. The second reason was the presence of GNPs that filled pores at the nanoscale level.

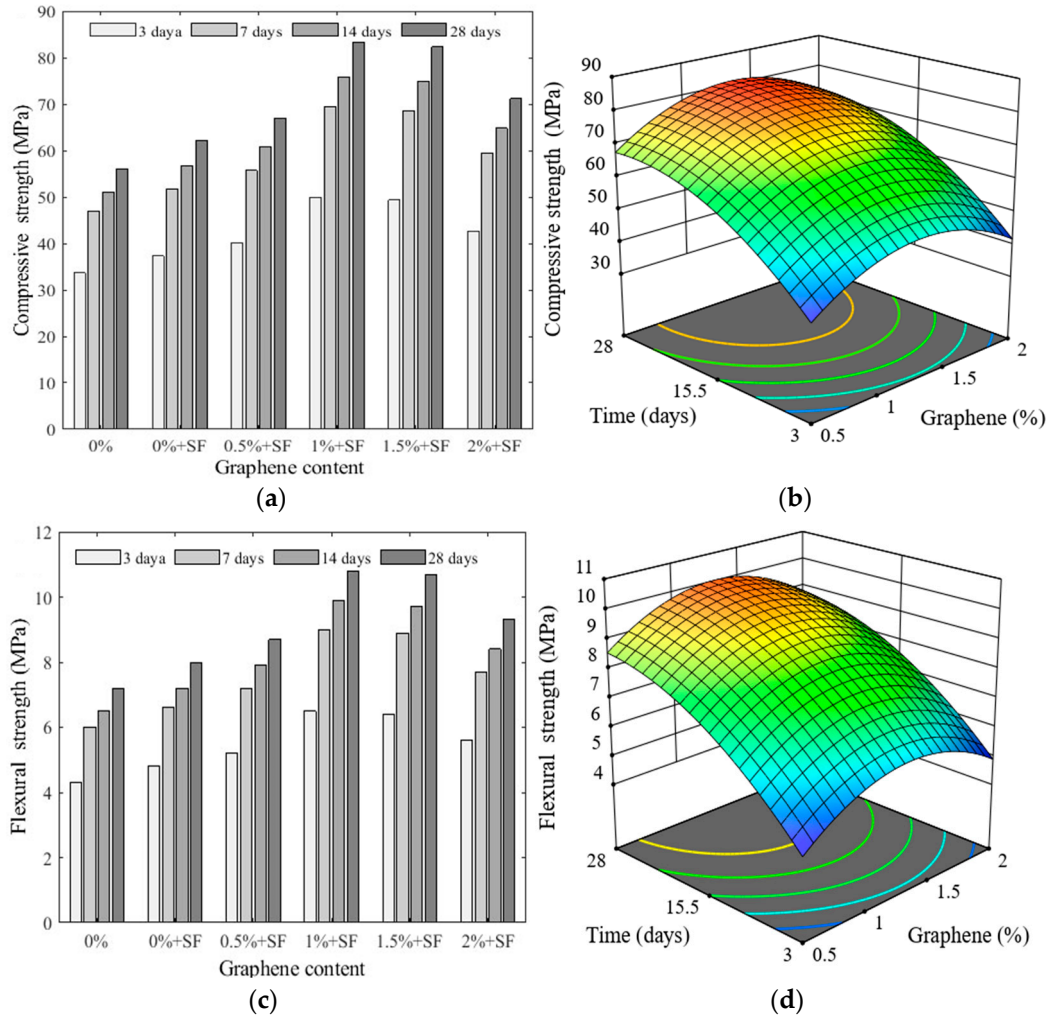

Figure 5. Actual and predicted strength of mortar: (**a**) compressive strength; (**b**) compressive strength; (**c**) flexural strength, and (**d**) flexural strength.

3.2. Microstructure Analysis

Figure 6 illustrates SEM micrographs of the microstructure of one of the specimens containing GNPs, during cement hydration and the development of hydration products.

Unreacted particles inside the hydrated cement paste resulted from an insufficient hydration rate, preventing the concrete from achieving its intended strength. The percentages of GNPs in the mixes strengthened the concrete mixtures, and therefore, the formation of C-S-H and the chemical reaction between Portlandite ($Ca(OH)_2$) and silica in the silica fume together with GNPs. The SEM micrograph clearly showed the improvement in the strength and distribution of C-S-H gel in the hardened cement paste. Figure 6a,b show the concrete samples' microstructure with magnifications of 10 µm and 2 µm, respectively. It is clear that the inter-locking benefits of utilizing graphene to fill and improve the pores' size distribution will lead to an increase in the strength of the concrete, as reported by previous researchers [28].

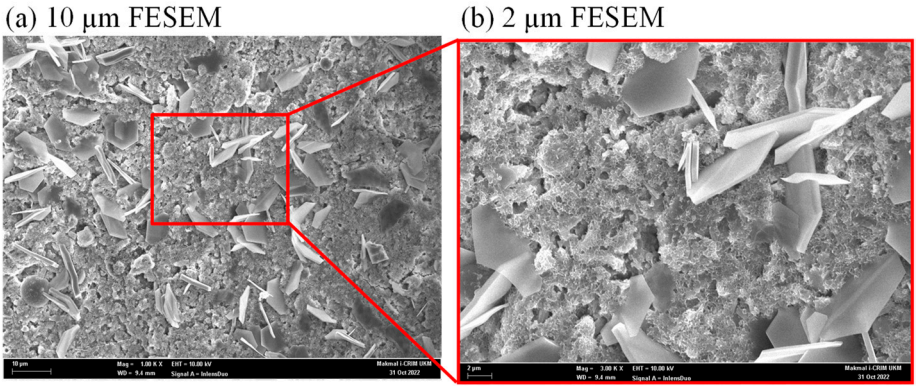

Figure 6. Image of FESEM test for the concrete specimen contains GNPs: (**a**) magnification of 10 µm, and (**b**) magnification of 2 µm.

The material characterization of the concrete samples after 28 days of the curing process with different graphene concentrations is illustrated in Figure 6. The EDX test was conducted for a greater understanding of the effect of GNPs on the microstructure characteristics of concrete. As shown in Figure 7a, the carbon concentration was low because the replacement of GNPs was at 0.5% regarding the replacement of the cement; the carbon content started to increase with the increasing content of GNPs, as shown in Figure 7b–d. The wall effect and nanofiller migration effect enriched the ITZ with nanofillers and affected the walls containing GNPs, which had an improvement on the microstructures in the ITZ [11]. Furthermore, when the 0-D, 1-D, and 2-D nanomaterials were added to the mixture, it could absorb a greater amount of water in the composite, leading to an improved capacity for decreasing the local water to binder content [29].

The 2-D nanomaterials can interact in two dimensions with much more calcium silicate hydrate (C-S-H), resulting in an additional comprehensive reinforcing effect compared to the 1-D nanomaterials [11,30].

3.3. Optimization Using RSM Model

Response surface methodology was also used to assess and determine the significance of independent parameters on the compressive strength of mortar, as shown in Figure 8a. A sharp slope gradient of GNPs content (d_0) was found to be recorded, thus confirming that the do was significant. The strength significantly increased, with increases of up to 1.3%. After that, a drop in compressive strength was reordered. This was in line with the results obtained from ANOVA, in which the *p*-value and F-value of the do were less than 0.0958 and 5.76, respectively. This result confirmed that the impact of graphene content on mortar strength was significant. In addition, the time (d_1) content was also considered significant due to the slope gradient, which increased with the increase of the curing duration.

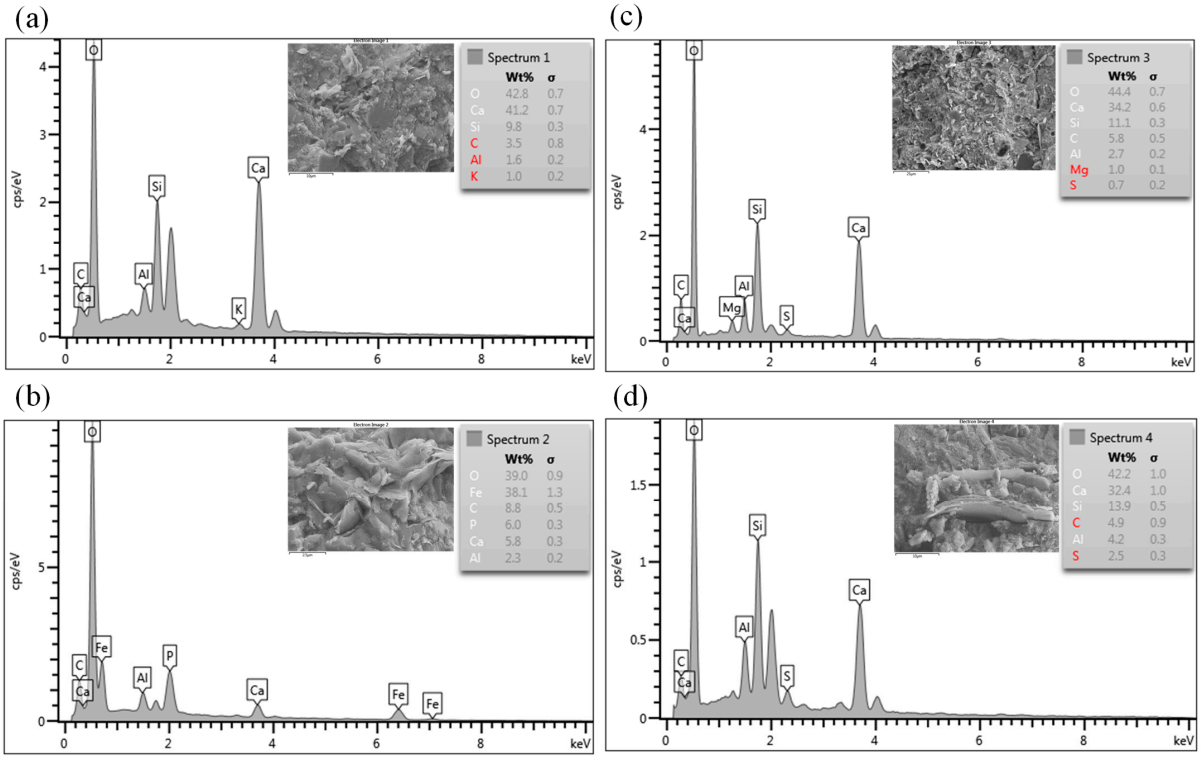

Figure 7. Image of EDX test for the concrete specimen contains GNPs: (**a**) 0.5% GNPs of 10 µm; (**b**) 1% GNPs; (**c**) 1.5% GNPs, and (**d**) 2% GNPs.

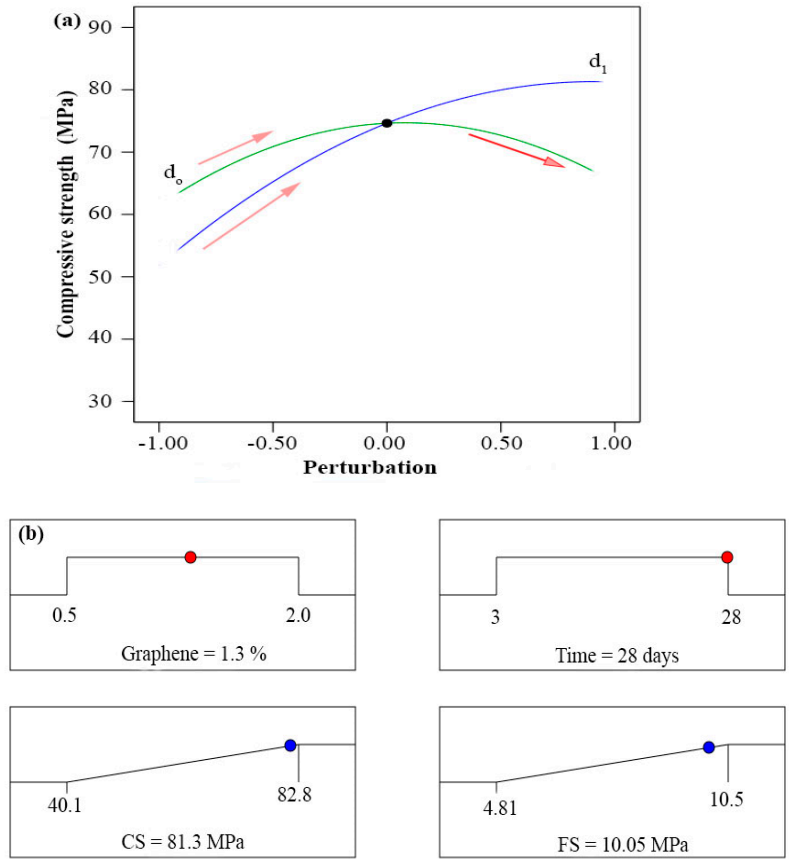

Figure 8. Evolution of mortar strength and their parameters (**a**) significant of the independent parameters on strength (**b**) optimization of the independent parameters.

Desirability functions provided by the RSM model were also taken into account to optimize the influential factors on the compressive strength and flexural strength, as shown in Equations (7) and (8) respectively. According to the solutions of the desirability functions, the best and most optimal influential factors were presented in Figure 8b. It can be seen that the optimal concentration of GNPs was 1.3% for both compressive and flexural strength tests.

4. Conclusions

The present study evaluates the performance of graphene-based mortar incorporating silica fume based on compressive and flexural strength. The RSM model was also used to predict and optimize the mortar properties. According to the experimental and predicted results, the following conclusions can be drawn:

I. The optimum mortar mixture was designed with a cement-to-sand ratio of 1:1.5 by mass and a water-cement ratio of 0.32, which was effective in achieving the target strength (more than 80 MPa).
II. The highest mechanical properties were achieved when the graphene content was 1.5%, and when the cement replaced by silica fume was 10%.
III. Increasing the content of GNPs by more than 1.5% caused a reduction in compressive and flexural strength.
IV. The presence of nanographene flakes showed their ability to fill the mortar pores, which was supported by FESEM. The sharp hexagon shapes of the GNPs have appeared and played a significant role in improving the concrete.
V. The RSM model showed its ability to predict accurate results in which MAPE and SI were less than 0.11. The RSM model also showed a strong correlation between the predicted and experimental results in which R^2 is greater than 0.9.

Author Contributions: Writing—original draft, H.A.S. and H.A.A.; Software, H.A.S. and H.A.A.; Supervision, A.A.M.; Data curation, A.A.M.; Writing—review & editing, H.A.S., N.S., M.E. and H.A.A.; Formal analysis, H.A.A. and M.E.; Resources, H.A.S.; Validation, I.B.Y. and M.A.I.Y.; Visualization, I.B.Y.; Methodology, M.A.I.Y. All authors have read and agreed to the published version of the manuscript.

Funding: This research was funded by the Center For Research Management and Instrumentation (CRIM), and Dana Impak Perdana with a grant number DIP-2021-014.

Institutional Review Board Statement: Not applicable.

Informed Consent Statement: Not applicable.

Data Availability Statement: The data presented in this study are available on request from the corresponding author.

Acknowledgments: In order to get the intended results, the authors would like to thank Universiti Kebangsaan Malaysia (UKM) for financing and supporting this study.

Conflicts of Interest: The authors declare no conflict of interest or so on for the publication of the review paper.

References

1. Wang, B.; Gupta, R. Analyzing bond-deterioration during freeze-thaw exposure in cement-based repairs using non-destructive methods. *Cem. Concr. Compos.* **2021**, *115*, 103830. [CrossRef]
2. Algaifi, H.A.; Bakar, S.A.; Alyousef, R.; Sam, A.R.M.; Alqarni, A.S.; Ibrahim, M.H.W.; Shahidan, S.; Ibrahim, M.; Salami, B.A. Machine learning and RSM models for prediction of compressive strength of smart bio-concrete. *Smart Struct. Syst.* **2021**, *28*, 535–551.
3. Chetty, K.; Watson, M.; Raine, T.; McGurgan, T.; Ladislaus, P.; Chen, J.; Zhang, S.; Lin, L.; Jiang, G. Enhancing Concrete and Mortar Properties and Durability Using Pristine Graphene Particles. *Coatings* **2022**, *12*, 1703. [CrossRef]
4. Feng, H.; Chen, G.; Gao, D.; Zhao, K.; Zhang, C. Mechanical properties of steel fiber-reinforced magnesium phosphate cement mortar. *Adv. Civ. Eng.* **2018**, *2018*, 3978318. [CrossRef]

5. Mu, R.; Li, H.; Qing, L.; Lin, J.; Zhao, Q. Aligning steel fibers in cement mortar using electro-magnetic field. *Constr. Build. Mater.* **2017**, *131*, 309–316. [CrossRef]
6. Dawood, E.T.; Ramli, M. High strength characteristics of cement mortar reinforced with hybrid fibres. *Constr. Build. Mater.* **2011**, *25*, 2240–2247. [CrossRef]
7. Khan, M.; Jamil, M.; Karim, M.R.; Zain, M.F.M.; Kaish, A.B.M.A. Filler effect of pozzolanic materials on the strength and microstructure development of mortar. *KSCE J. Civ. Eng.* **2017**, *21*, 274–284. [CrossRef]
8. Al-Jabri, K.; Shoukry, H. Use of nano-structured waste materials for improving mechanical, physical and structural properties of cement mortar. *Constr. Build. Mater.* **2014**, *73*, 636–644. [CrossRef]
9. Rao, S.; Silva, P.; De Brito, J. Experimental study of the mechanical properties and durability of self-compacting mortars with nano materials (SiO_2 and TiO_2). *Constr. Build. Mater.* **2015**, *96*, 508–517. [CrossRef]
10. Alnahhal, W.; Taha, R.; Al-Nasseri, H.; Nishad, S. Effect of using Cement Kiln Dust as a nano-material on the strength of cement mortars. *KSCE J. Civ. Eng.* **2018**, *22*, 1361–1368. [CrossRef]
11. Wang, X.; Dong, S.; Ashour, A.; Zhang, W.; Han, B. Effect and mechanisms of nanomaterials on interface between aggregates and cement mortars. *Constr. Build. Mater.* **2020**, *240*, 117942. [CrossRef]
12. Kumar, P.; Huo, P.; Zhang, R.; Liu, B. Antibacterial properties of graphene-based nanomaterials. *Nanomaterials* **2019**, *9*, 737. [CrossRef]
13. Liu, J.; Fu, J.; Yang, Y.; Gu, C. Study on dispersion, mechanical and microstructure properties of cement paste incorporating graphene sheets. *Constr. Build. Mater.* **2019**, *199*, 1–11. [CrossRef]
14. Shamsaei, E.; de Souza, F.B.; Yao, X.; Benhelal, E.; Akbari, A.; Duan, W. Graphene-based nanosheets for stronger and more durable concrete: A review. *Constr. Build. Mater.* **2018**, *183*, 642–660. [CrossRef]
15. Li, X.; Li, C.; Liu, Y.; Chen, S.J.; Wang, C.; Sanjayan, J.; Duan, W.H. Improvement of mechanical properties by incorporating graphene oxide into cement mortar. *Mech. Adv. Mater. Struct.* **2018**, *25*, 1313–1322. [CrossRef]
16. Wang, Q.; Wang, J.; Lu, C.-X.; Liu, B.-W.; Zhang, K.; Li, C.-Z. Influence of graphene oxide additions on the microstructure and mechanical strength of cement. *New Carbon Mater.* **2015**, *30*, 349–356. [CrossRef]
17. Amini, K.; Amiri, S.S.; Ghasemi, A.; Mirvalad, S.; Korayem, A.H. Evaluation of the dispersion of metakaolin–graphene oxide hybrid in water and cement pore solution: Can metakaolin really improve the dispersion of graphene oxide in the calcium-rich environment of hydrating cement matrix? *RSC Adv.* **2021**, *11*, 18623–18636. [CrossRef]
18. Zhai, S.; Pang, B.; Liu, G.; Zhang, Y.; Xu, K.; She, W.; Zhang, Y. Investigation on preparation and multifunctionality of reduced graphene oxide cement mortar. *Constr. Build. Mater.* **2021**, *275*, 122119. [CrossRef]
19. Kiamahalleh, M.V.; Gholampour, A.; Tran, D.N.; Ozbakkaloglu, T.; Losic, D. Physiochemical and mechanical properties of reduced graphene oxide–cement mortar composites: Effect of reduced graphene oxide particle size. *Constr. Build. Mater.* **2020**, *250*, 118832. [CrossRef]
20. Sajjad, U.; Sheikh, M.; Hadi, M. Experimental study of the effect of graphene on properties of ambient-cured slag and fly ash-based geopolymer paste and mortar. *Constr. Build. Mater.* **2021**, *313*, 125403. [CrossRef]
21. Jiang, Z.; Sherif, M.M.; Xing, G.; Ozbulut, O.E. Tensile characterization of graphene nanoplatelets (GNP) mortar using acoustic emissions. *Mater. Today Commun.* **2020**, *25*, 101433. [CrossRef]
22. Al-Fasih, M.Y.M.; Huseien, G.E.; bin Ibrahim, I.S.; Sam, A.R.M.; Algaifi, H.A.; Alyousef, R. Synthesis of rubberized alkali-activated concrete: Experimental and numerical evaluation. *Constr. Build. Mater.* **2021**, *303*, 124526. [CrossRef]
23. Tay, Y.W.D.; Qian, Y.; Tan, M.J. Printability region for 3D concrete printing using slump and slump flow test. *Compos. Part B Eng.* **2019**, *174*, 106968. [CrossRef]
24. Carrillo, J.; Ramirez, J.; Lizarazo-Marriaga, J. Modulus of elasticity and Poisson's ratio of fiber-reinforced concrete in Colombia from ultrasonic pulse velocities. *J. Build. Eng.* **2019**, *23*, 18–26. [CrossRef]
25. Mohammed, B.S.; Khed, V.; Nuruddin, M. Rubbercrete mixture optimization using response surface methodology. *J. Clean. Prod.* **2018**, *171*, 1605–1621. [CrossRef]
26. Gong, Y.; Song, J.; Lin, S.; Yang, J.; He, Y.; Tan, G. Design optimization of rubber-basalt fiber-modified concrete mix ratios based on a response surface method. *Appl. Sci.* **2020**, *10*, 6753. [CrossRef]
27. Hou, D.; Chen, D.; Wang, X.; Wu, D.; Ma, H.; Hu, X.; Zhang, Y.; Wang, P.; Yu, R. RSM-based modelling and optimization of magnesium phosphate cement-based rapid-repair materials. *Constr. Build. Mater.* **2020**, *263*, 120190. [CrossRef]
28. Dung, N.T.; Su, M.; Watson, M.; Wang, Y. Effects of using aqueous graphene on behavior and mechanical performance of cement-based composites. *Constr. Build. Mater.* **2023**, *368*, 130466. [CrossRef]
29. Han, B.; Ding, S.; Wang, J.; Ou, J. *Nano-Engineered Cementitious Composites*; Springer Nature: Singapore, 2019. [CrossRef]
30. Wang, X.; Dong, S.; Li, Z.; Han, B.; Ou, J. Nanomechanical Characteristics of Interfacial Transition Zone in Nano-Engineered Concrete. *Engineering* **2022**, *17*, 99–109. [CrossRef]